Journal of Power Sources 246 (2014) 299–304

Contents lists available at ScienceDirect

Journal of Power Sources

journal homepage: www.elsevier.com/locate/jpowsour

Short communication

A non-conventional fluorinated separator in high-voltage graphite/$LiNi_{0.4}Mn_{1.6}O_4$ cells

C. Arbizzani [a], F. Colò [a], F. De Giorgio [a], M. Guidotti [a], M. Mastragostino [a,*], F. Alloin [b], M. Bolloli [b], Y. Molméret [b], J.-Y. Sanchez [b]

[a] Alma Mater Studiorum Università di Bologna, Dipartimento di Chimica "Giacomo Ciamician", via Selmi 2, 40126 Bologna, Italy
[b] LEPMI, UMR 5279, CNRS, Grenoble INP, Université Joseph Fourier, Université de Savoie, 1130 rue de la piscine, 38402 Saint-Martin d'Hères, France

HIGHLIGHTS

- Graphite/LNMO cells with new pVDF–NCC and LF30 electrolyte with additives were tested.
- Beneficial impact of the pVDF–NCC separator on performance of high-voltage LIBs.
- HPPC tests of graphite/LNMO cells for power-assist HEV were performed.

ARTICLE INFO

Article history:
Received 15 April 2013
Received in revised form
18 July 2013
Accepted 25 July 2013
Available online 3 August 2013

Keywords:
pVDF–NCC separator
High-voltage lithium-ion battery
$LiNi_{0.4}Mn_{1.6}O_4$
LF30 electrolyte
Power-assist HEV
FreedomCAR test

ABSTRACT

Graphite/$LiNi_{0.4}Mn_{1.6}O_4$ cells assembled with a new reinforced polyvinylidene fluoride (pVDF)–nano crystalline cellulose (NCC) separator and EC–DMC 1 M LiFAP electrolyte with additives were tested by deep charge/discharge cycles at different C-rates and by the FreedomCAR DOE protocol to simulate the dynamic functioning of the batteries in power-assist full hybrid electric vehicles (HEVs). The results of this study evidence the beneficial impact of the pVDF–NCC macroporous membrane with respect to the polypropylene monolayer Celgard®2400 separator on the high C-rate cell performance. The deep charge/discharge of the cell with pVDF–NCC at C/1 effective rate provided 101 W h kg^{-1} to be compared with 85 W h kg^{-1} of the cell with Celgard®2400 (the cell weight was considered twice the composite electrode weight of both electrodes). Also hybrid pulse power characterization tests based on the FreedomCAR protocol at 5 C and 10 C demonstrated the superior performance of the cells with pVDF–NCC with respect to that of the cells with Celgard®2400 even if both cells exceed the FreedomCAR goals of power and energy for minimum and maximum power-assist HEV.

1. Introduction

High voltage cathode materials play a key role for the development of next generation high energy and power rechargeable Li-ion batteries (LIBs) for the applications in sustainable transport. Nickel manganese spinel oxides, such as $LiNi_{0.5-y}Mn_{1.5+y}O_4$ ($y \leq 0.1$) [1–6] with high operating voltages can provide 5 V LIBs featuring specific energy higher than 200 W h kg^{-1}. Notably, $LiNi_{0.4}Mn_{1.6}O_4$ for the high rate capability and stability has been identified as the most promising nickel manganese oxides [6]. We have recently investigated the performance of full cells having $LiNi_{0.4}Mn_{1.6}O_4$ (LNMO) and graphite electrodes with carbonate-based electrolyte, ethylene carbonate (EC)–dimethyl carbonate (DMC) with $Li[(C_2F_5)_3PF_3]$ (LiFAP), a non conventional lithium salt, even in presence of SEI-forming additives, and commercial Celgard®2400 separator, which is a polypropylene (PP)-monolayer [7].

In LiBs the separator is an important component for cell performance and it is also crucial for cell safety [8]. Celgard®2400 is a semi-crystalline microporous polymer and, below the melting temperature, displays high mechanical strength so that thin films are feasible. Besides the thermomechanical properties, electrolyte-soaked separators should retain as much as possible the same conductivity and chemical/electrochemical stability versus both electrodes of the neat electrolyte. Tortuosity of the insulating polymeric matrix increases the length of the ion path and, hence, decreases the conductivity. Porosity affects separator conductivity and it must be emphasized that the wetting of the pores of apolar polyolefins by polar electrolytes like those based on EC:DMC is unfavoured because of the poor polymer–solvent interactions. Some properties of Celgard®2400 are described in Ref. [9].

Polyvinylidene fluoride (pVDF) is often used as binder for both electrodes and pVDF separators, early proposed by Boudin et al.

* Corresponding author.
E-mail address: marina.mastragostino@unibo.it (M. Mastragostino).

0378-7753/$ – see front matter © 2013 Elsevier B.V. All rights reserved.
http://dx.doi.org/10.1016/j.jpowsour.2013.07.095

[10], were successfully used in LIBs with EC–DMC based electrolytes [11–13] because of the good electrode/electrolyte contact. However, the strong affinity between pVDF and carbonate-based electrolytes sharply decreases the separator mechanical strength [14]. The blending of polymers with nano crystalline cellulose (NCC) was an effective strategy to reinforce polymer electrolytes: the NCC, because of its high aspect ratio provides with low percolation threshold a network through hydrogen bonding involving surface –OH groups [15].

These features are interesting premises to improve performance of the graphite/LNMO cells operating with EC–DMC 1 M LiFAP electrolyte in presence of additives, and the aim of the present paper is to highlight the effect of a new reinforced pVDF–NCC macroporous separator in such cells. The results of electrochemical tests performed both by deep charge/discharge cycles at different C-rates and by the FreedomCAR DOE protocol to simulate the dynamic functioning of the batteries in power-assist full HEVs [16] are reported and compared to those of cells with Celgard®2400.

2. Experimental

The preparation of pVDF–NCC membranes was carried out by a phase inversion process. NCC (FP Innovation) was added to dimethylformamide and an NCC dispersion was prepared by Ultraturrax mixer and ultrasonic device; pVDF (Solef®6020, Solvay) was then dissolved in the NCC dispersion to obtain a homogeneous slurry. The phase inversion protocol was performed using an ethanol bath and the membranes were then dried under vacuum (2 mm Hg) at 60 °C to further remove any trace of solvent, and stored in glove box. The amount of NCC in the new reinforced pVDF–NCC separator used in this study was 8 wt%.

Full cells having positive electrodes based on $LiNi_{0.4}Mn_{1.6}O_4$ (LNMO) made by CEA (Grenoble) and graphite-based negative electrodes were assembled. Composition (in wt%) of the positive electrodes was 85% LNMO, 10% Super C65 (TIMCAL) conductive carbon and 5% pVDF (Solef®5130, Solvay) binder and that of the graphite electrodes was 89% graphite (SLA-1025, Superior Graphite Co.), 3% PureBLACK™ (Superior Graphite, Co.) conducting additive and 8% pVDF (Solef® 5130, Solvay). The electrode mass balancing in the full cells was made by setting the ratio of the capacity of the negative to that of the positive near 1. The active material mass loading was 7.7 for the cathode and 3.0 mg cm^{-2} for the anode. LNMO electrodes were pressed at 1500 psi and graphite electrodes were roll pressed; disk electrodes (0.64 cm^2) were dried at 120 °C for 12 h under vacuum before use. Cell assembly was performed in an MBraun Labmaster SP glove box (water and oxygen content <0.1 ppm) using the new macroporous pVDF–NCC membrane (18 μm) or the commercial PP membrane (Celgard®2400, 25 μm) as separators. The electrolyte was EC:DMC 1:1–1 M lithium tris(pentafluoroethyl)trifluoroposphate (LF30, Merck, water ≤20 ppm and HF content ≤50 ppm) with additives (unless otherwise indicated). The additives were monofluoroethylene carbonate (F1EC, Solvay Fluor, purity ≥99.9 wt%, water and HF content ≤20 ppm) and succinic anhydride (SA, Sigma–Aldrich, purity ≥99%), used as received, and their amount in the electrolyte solutions was 1.6 wt% and 2 wt%, respectively.

The discharge and charge capability tests on the full cells were performed utilizing Swagelok™-type cells in two-electrode configuration at 30 °C. Such cells had a Li reference electrode to check, in case, the potential of each electrode. Supplementary material Fig. S1 shows cell and electrode voltage profiles of charge/discharge at 0.1 C of a graphite//LNMO cell with pVDF–NCC separator at 30 °C before static capacity tests of FreedomCAR protocol carried out in three-electrode configuration. The tests were carried out by a Biologic VMP multichannel potentiostat/galvanostat and the temperature was controlled by a Memmert IPP 200 oven.

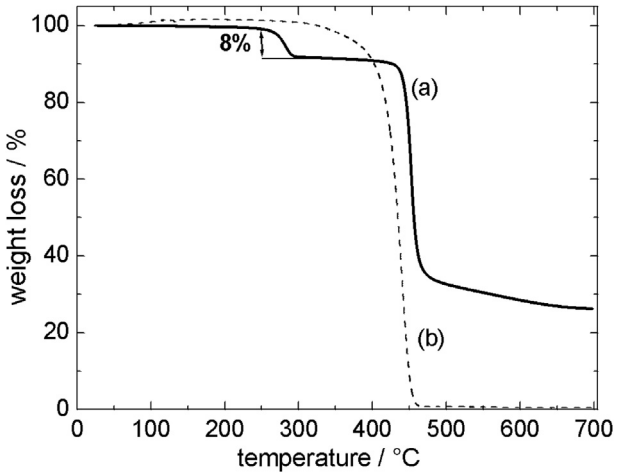

Fig. 1. Thermogravimetric analysis of dry separators (a) pVDF–NCC and (b) Celgard®2400, in Ar flux (5 °C min^{-1}).

Impedance spectroscopy (IS) measurements of electrolyte-soaked macroporous pVDF–NCC and Celgard separators were carried out with stainless steel blocking electrodes (0.785 cm^2) and those of the full cells were performed in open circuit conditions using a Solartron SI 1255 frequency response analyzer coupled with a 273 A PAR potentiostat/galvanostat. An ac amplitude of 5 mV was used and data were collected taking 10 points per decade. The linear sweep voltammetries (LSVs) of separators in LF30 were carried out with a Swagelok™-type cell in three-electrode configuration at 30 °C with stainless steel electrodes as working and counter electrodes and Li metal as reference. The differential thermal analysis (DTA) of dry separators was carried out with a Linseis L6310, the thermo-gravimetric analysis (TGA) with a TA Instruments Q50 and scanning electron microscopy (SEM) images with a Zeiss EVO 50.

3. Results and discussion

3.1. Preparation and characterization of pVDF–NCC separator

The preparation of the reinforced pVDF–NCC macroporous membrane was performed by a phase inversion procedure described

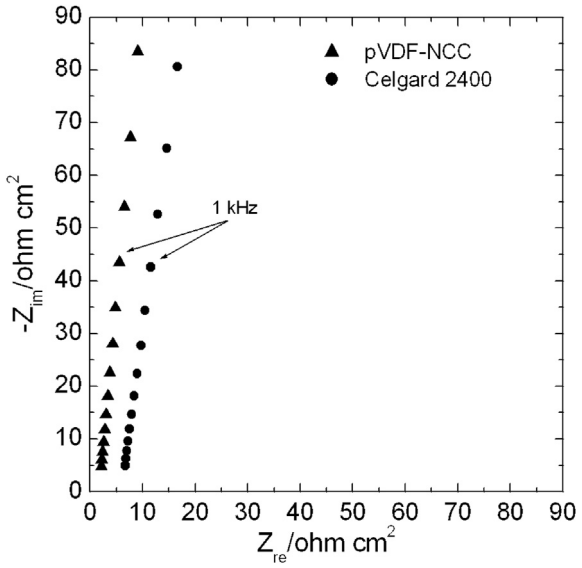

Fig. 2. IS spectra of the electrolyte-soaked pVDF–NCC and Celgard®2400 separators at 30 °C (10 kHz to 0.5 kHz).

in Experimental section. Fig. 1 displays the TGA in Ar atmosphere of the pVDF–NCC membrane from 30° to 700 °C and evidences a first weight loss in the temperature range 260–300 °C corresponding to 8 wt% due to thermal decomposition of NCC; hence, the weight remains constant up to 430 °C at which the pVDF decomposition starts. Fig. 1 also displays the TGA of Celgard®2400 for comparison of the thermal stability.

The electrolyte-soaked membrane resistances were evaluated by IS at 30 °C with stainless steel blocking electrodes. The Nyquist diagram of Fig. 2 shows that the resistance values per cm^2 at 1 kHz are 5.6 and 11.6 Ω cm^2 for pVDF–NCC and Celgard®2400, respectively, indicating that the reinforced pVDF–NCC membrane will give a lower contribution to cell resistance than Celgard®2400. The MacMullin number, N_m, i.e. the ratio of resistivity of the electrolyte-soaked separator to that of the electrolyte, which is related to membrane's porosity and tortuosity, evaluated for both membranes, by taking into account their thickness, from the intercepts on the *x*-axis of the plots in Fig. 2 and the electrolyte resistivity of 1.2×10^2 Ω cm, was 6 for pVDF–NCC membrane and 16 for Celgard; hence, the pVDF–NCC separator will affect battery performance at high C-rate less than Celgard. The higher porosity of pVDF–NCC membrane than that of Celgard®2400 is clearly evidenced by SEM images (Fig. S2 in Supplementary material).

Separator is an important component for battery safety. In abuse conditions as the cell temperature increases the separator should close the pores to stop ionic transport (shutdown) and then the current flow, still maintaining a good mechanical integrity to avoid an internal short circuit. Fig. 3a shows the logarithm of the real part of impedance, Z_{re}, at 1 kHz *vs.* temperature of the electrolyte-soaked pVDF–NCC. The resistance greatly increases at the temperature at which the pores collapse and the membrane become an "insulator", i.e. at the shutdown temperature which generally corresponds to the polymer melting temperature. It is worth noting that after the polymer melting the resistance remains high thus indicating good melt integrity up to 220 °C, which is a temperature well above the required minimum melt integrity temperature of 150 °C. Fig. 3b shows the shutdown behaviour for Celgard®2400, and the results are comparable to those with pVDF–NCC separator. The insets in the figures display the melting temperatures of both separators and evidence that while shutdown and melting temperatures for Celgard correspond, the shutdown temperature for pVDF–NCC is ca. 10° higher than melting, presumably for the macroporous nature of this reinforced membrane. Further details about pVDF–NCC characterizations are in Ref. [17].

The electrochemical stability to oxidation and reduction of the pVDF–NCC membrane has been investigated by LSV in a three electrode cell with LF30 electrolyte without additives, and Fig. S3 in Supplementary material shows the second LSV at 5 mV s^{-1} towards oxidation and reduction potentials; for a comparison the figure displays the LSVs of Celgard®2400. In both cells the anodic limit, as the cathodic one, is restricted by the electrolyte. Hence, the pVDF–NCC membrane, as Celgard, is stable at high oxidation potential and may be used in high voltage lithium ion batteries.

3.2. Electrochemical tests on graphite/LNMO cells

The electrochemical characterization of the full cells with macroporous pVDF–NCC separator saturated with LF30 and additives involved deep charge/discharge cycles to estimate the discharge and charge capability of the cells, self-discharge tests and tests for HEV applications according to the standards stated by U.S. Department of Energy (DOE) in Ref. [16], including static capacity (SC) tests and hybrid pulse power characterization (HPPC) tests.

The deep charge/discharge cycles were performed by the following protocol: charge at C/10 up to 4.95 V, open circuit condition

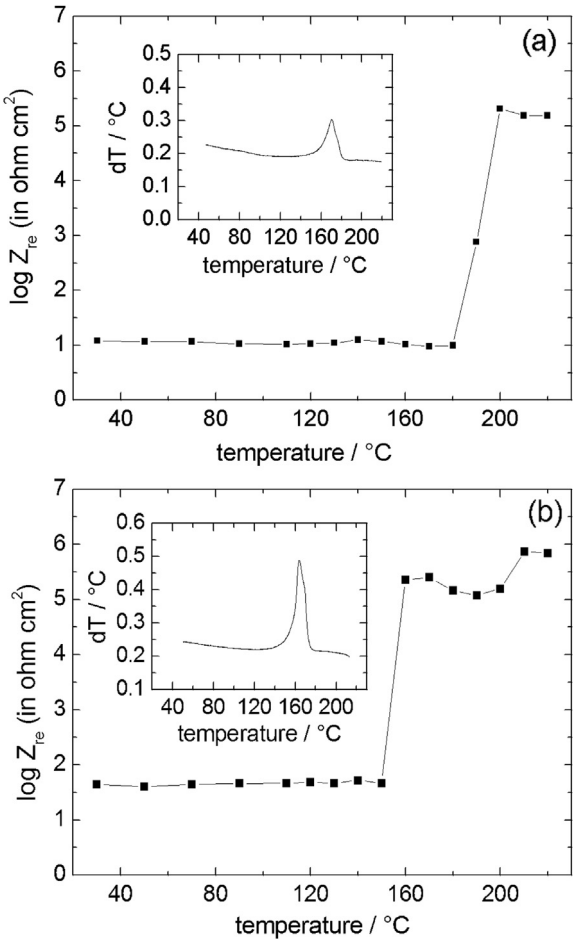

Fig. 3. Logarithm Z_{re}, at 1 kHz *vs.* temperature over shutdown tests of electrolyte-soaked separators (a) pVDF–NCC and (b) Celgard®2400. Insets display the DTA traces (5 °C min^{-1}) of dry separators.

(OCV) 0.5 h and discharges at different C-rates from C/10 to 2 C (4 cycles at each discharge C-rate, with exclusion of C/10) down to 3.5 V to evaluate the discharge capability; similarly, the test to evaluate the charge capability involved charges at different C-rates from C/10 to 2 C, OCV 0.5 h and discharge at C/10. At the end, additional 2 charge/discharge cycles at C/10 (including 0.5 h OCV) were performed to estimate the capacity retention, i.e. the ratio between the discharge capacity of the last C/10 cycle (46th cycle) and that of the 1st one. Furthermore, impedance measurements on the cell in the discharged state at 24th cycle (i.e. at the beginning of the charge capability tests) and at 46th cycle (i.e. at the end of the charge capability tests) were performed. Fig. 4 compares the results of these tests on cells with pVDF–NCC (circle) and Celgard®2400 (triangles) separators. The cell with the macroporous separator displays significantly higher capacities than that with Celgard®2400 at the highest C-rate and this is notably evident from the charge capability data (Fig. 4b). Moreover, the capacity retention of the cell with pVDF–NCC separator is 63% and that of the cell with Celgard 47%.

The pVDF–NCC membrane providing a better compatibility with the electrodes, which have pVDF binder, than Celgard®2400 gives a lower and more stable ion transport resistance which reflects positively on the battery performance at high C-rate. This is also supported by the impedance data at 1 kHz recorded at the beginning and the end of charge capability tests on the discharged cells with the two separators: while the Z_{re} value of the cell with pVDF–NCC membrane remained constant at 17 Ω cm^2 that of the cell with Celgard®2400 increased from 41 to 57 Ω cm^2.

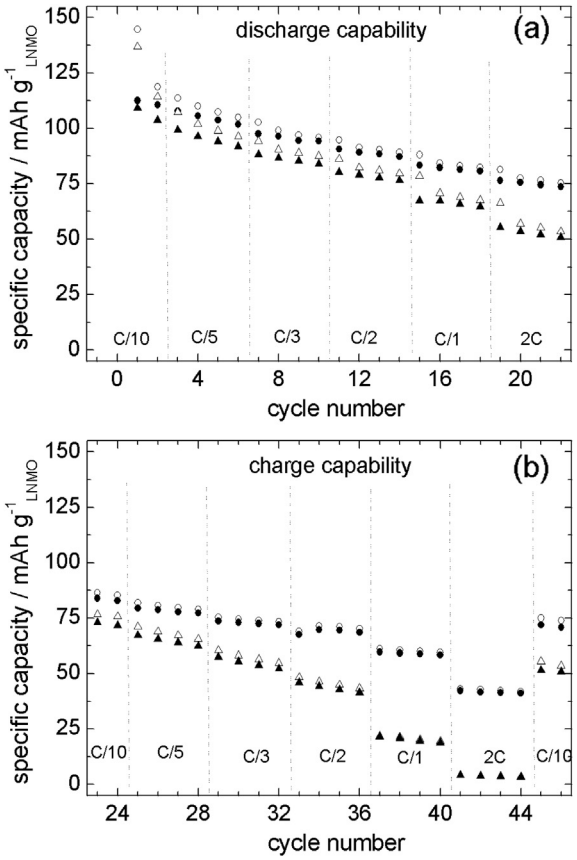

Fig. 4. Comparison of discharge (a) and charge (b) capability of cells with pVDF–NCC (circle) and Celgard®2400 separator (triangles). Charge is indicated by void and discharges by full symbols.

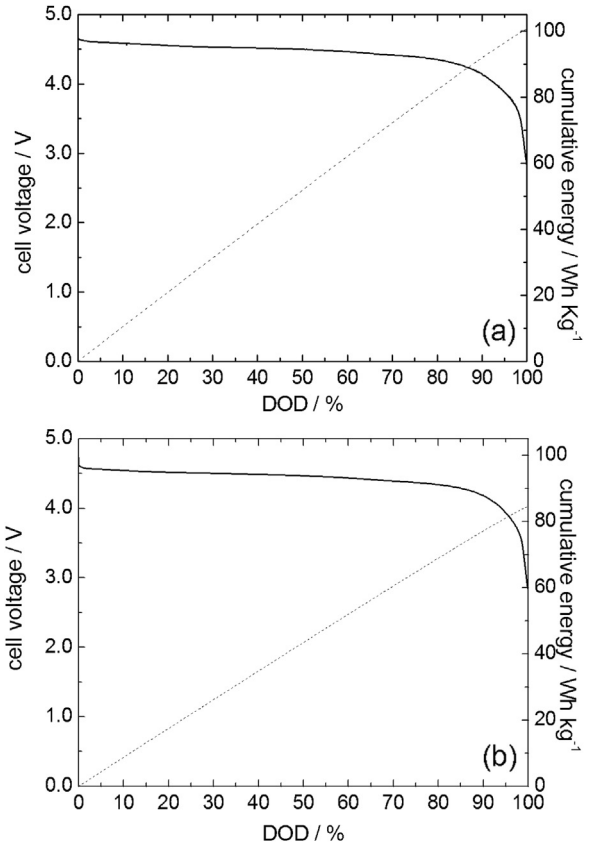

Fig. 5. Discharge voltage profile (solid line) and delivered specific energy (dashed line) at C/1 effective rate *vs.* DOD of the cells with (a) pVDF–NCC and (b) Celgard®2400.

The self-discharge test on the cells involved full charge at C/10, 20 h in OCV condition and discharge at C/10 to evaluate the recovered charge after 20 h, and this sequence was repeated for 13 times. The percentages of recovered charge at the 2nd and at the last sequence of the cell with pVDF–NCC separator were 87% and 84%, respectively, whereas those of the cell with Celgard were 83% and 80%.

The SC tests on full cells with the two separators were performed by C/1 effective discharge-rate, at 30 °C, to evaluate the energy removed from the cells (after charge up to 4.75 V) at different depth of discharge (DOD), and the results are shown in Fig. 5. Herein after (Fig. 5 included) all the specific parameters (energy and power) refer to a total battery weight which is twice the composite electrode weight of both electrodes, as to include the weight contribution of all the other battery components according to Ref. [18]. Fig. 5a shows that the cumulative energy removed from the cell with pVDF–NCC membrane is 101 W h kg^{-1}, a higher value than that removed from the cell with Celgard, 85 W h kg^{-1}, shown in Fig. 5b, as expected after the above reported discharge and charge capability results.

The HPPC tests, that incorporate 10 s discharge and regenerative constant current pulses and 40 s rest between the two pulses, performed at different DOD from 10% to 90%, separated by 10% DOD segments at C/1 constant rate and 1 h equilibration time (rest time), were carried out on cells with the two separators at low (5 C) and high discharge rate (10 C) with regenerative currents which were 75% of those of the discharge. The test ends before 90% DOD if the cell voltage exceeds the selected $V_{max} = 5.1$ V in regenerative pulse and $V_{min} = 0.55V_{max}$ in discharge pulse. Fig. 6 shows the HPPC voltage profile of the cell with pVDF–NCC membrane along the sequence from 10% to 90% DOD with discharge pulses at 5 C (2.25 mA cm^{-2}) at 30 °C; the plot also shows the voltage during the rest time before the beginning of the test. The inset in the figure displays the magnification of the pulses at 10% DOD, as an example, to mark the cell voltage values just before the discharge and regenerative pulses, V_0 and V_2, and those at the end of these pulses, V_1 and V_3, which were used to calculate at each %DOD the discharge and regenerative pulse resistances, R_{dis} and R_{reg}, by Eqs. (1) and (2)

$$R_{dis} = (V_1 - V_0)/I_{dis} \quad (1)$$

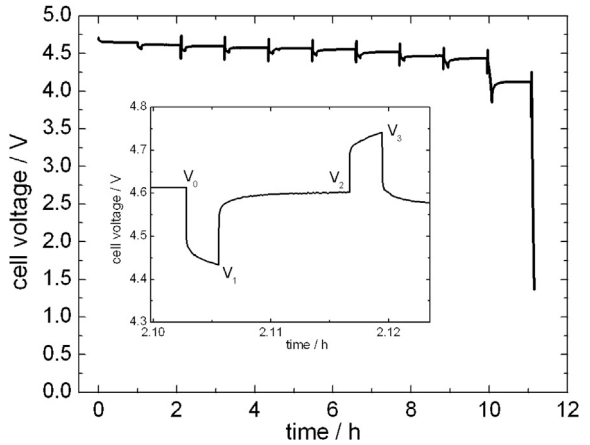

Fig. 6. Cell voltage profile over HPPC at 5 C of the cell with pVDF–NCC separator. In the inset, the magnification of the discharge and regenerative pulses at 10% DOD.

$$R_{reg} = (V_3 - V_2)/I_{reg} \quad (2)$$

and, then, the discharge and regenerative pulse-power, P_{dis} and P_{reg}, by Eqs. (3) and (4)

$$P_{dis} = V_{min}(V_0 - V_{min})/R_{dis} \quad (3)$$

$$P_{reg} = V_{max}(V_{max} - V_2)/R_{reg} \quad (4)$$

Fig. 7a reports the R_{dis} and R_{reg} values by the low and high current HPPC tests (the 10 C test ended at 60% DOD) and Fig. 7b the specific power values (discharge and regenerative) by the 5 C current tests *vs.*

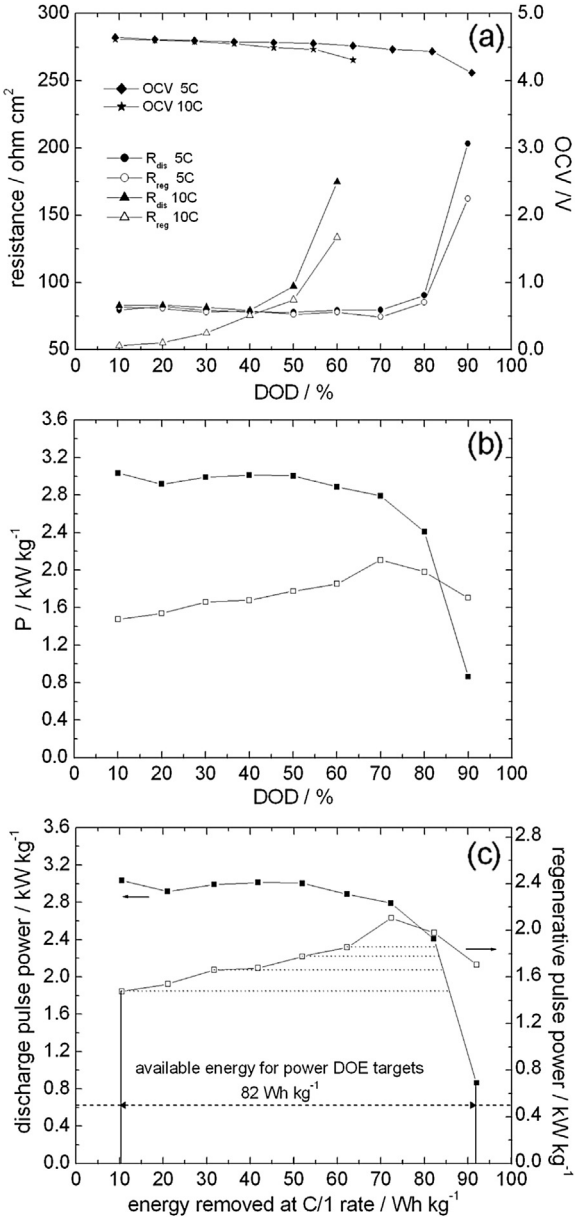

Fig. 7. Cell with pVDF–NCC separator: (a) open circuit voltage and resistance from discharge (full symbol) and regenerative (void symbol) pulses *vs.* DOD% from HPPC tests at 5 C and 10 C (the last ends at 60% DOD); (b) specific power of discharge (full symbol) and regenerative (void symbol) pulses from HPPC test at 5 C *vs.* DOD%; (c) specific discharge power (full symbol) and regenerative power (void symbol) from HPPC test at 5 C with the two vertical axes rescaled in proportion of discharge and regenerative power goals *vs.* energy removed during C/1 discharge of Fig. 5a.

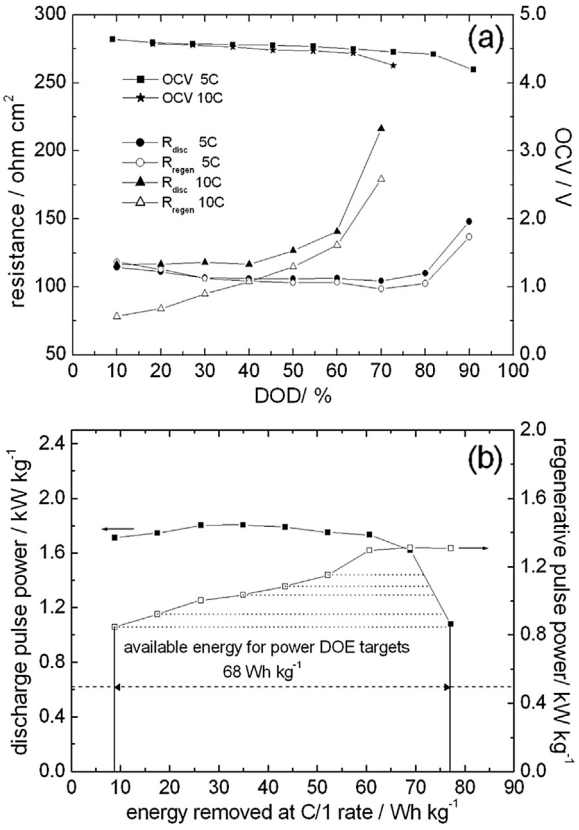

Fig. 8. Cell with Celgard®2400 separator: (a) open circuit voltage and resistance from discharge (full symbol) and regenerative (void symbol) pulses *vs.* DOD% from HPPC tests at 5 C and 10 C (the last ends at 70% DOD); (b) specific discharge power (full symbol) and regenerative power (void symbol) from HPPC test at 5 C with the two vertical axes rescaled in proportion of discharge and regenerative power goals *vs.* energy removed during C/1 discharge of Fig. 5b.

%DOD of the cell with pVDF–NCC separator. In order to evaluate the available energy, which is defined as the energy removed during a C/1 discharge over the DOD range for which the discharge and regenerative pulse power goals for a given mode (minimum or maximum power assist HEV) are precisely met, Fig. 7b is transformed in Fig. 7c through the data of Fig. 5a, and the two vertical axes are scaled in proportion to the discharge and regenerative power goals. The dashed horizontal line in Fig. 7c identify on *y*-axes the discharge and regenerative FreedomCAR power goals for the minimum power assist HEV expressed in terms of specific values (625 W kg^{-1} discharge and 500 W kg^{-1} regenerative power pulses) and calculated by dividing the FreedomCAR goals by the maximum weights of the battery pack. The FreedomCAR targets for all the electrochemical system are: discharge pulses of 25 and 40 kW, regenerative pulses of 20 and 35 kW, maximum weight of 40 and 60 kg and total available energy over DOD range where both power goals are met of 0.3 and 0.5 kW h at C/1 rate for the minimum and maximum power assist HEV, respectively.

The difference in the removed energy between the two vertical lines in Fig. 7c, 82 W h kg^{-1}, corresponds to the specific available energy for power pulses which meet the goals for minimum power assist HEV, and largely surpass the energy target of 7.5 W h kg^{-1}. Power pulses beyond these goals are viable with lower available energy, as indicated by the dotted segments between the discharge and regenerative pulse power curves.

Fig. 8 shows the results of the HPPC tests performed at 30 °C on full cells with Celgard separator: Fig. 8a reports the R_{dis} and R_{reg} values by the low and high current HPPC tests (the 10 C test ended

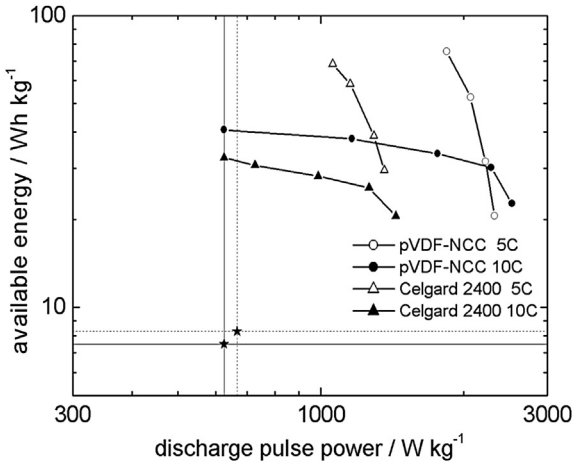

Fig. 9. Plots of the available energy for a given pulse-power *vs.* discharge pulse power for cells with pVDF and Celgard®2400 separators from HPPC test at 5 C and 10 C.

at 70% DOD) and Fig. 8b the specific power values (discharge and regenerative) by 5 C HPPC tests *vs.* energy removed during a C/1 discharge (through the use of Fig. 5b as made for Fig. 7c). The specific available energy for power pulses which meet the goals for minimum power assist HEV is 68 W h kg^{-1}, a value lower than that of the cell with pVDF–NCC separator, even if higher than energy DOE target. By low current HPPC test data in Figs. 7c and 8b, and by analogous results of high current HPPC tests (calculated by using experimental data in Fig. 5a and b), plots of available energy *vs.* discharge pulse power for the two cells with pVDF–NCC and Celgard®2400 separators were built-up and are shown in Fig. 9. These plots, from 5 C to 10 C HPPC tests, represent the energy (or power) available over the operating region where a specified power (or energy) demand can be met. The horizontal and vertical lines indicate FreedomCAR energy and power targets for minimum (solid) and maximum (dashed) power assist HEV which are largely exceeded by both cells with the different separators. However, the cell with pVDF–NCC performs significantly better than the cell with Celgard®2400 evidencing again the beneficial effect of the fluorinated reinforced macroporous membrane with respect to the conventional polyolefinic separator in the functioning of high voltage cells such as those with LNMO cathode.

4. Conclusions

The results of this study evidence the beneficial impact of the new macroporous fluorinated reinforced separator pVDF–NCC with respect to the PP monolayer Celgard®2400 separator on the high-rate performance of the cells operating with LNMO high voltage cathode and graphite anode in LF30 with additives. This is due, as expected, to a good electrode/electrolyte contact because pVDF was also used as binder for both positive and negative electrodes. The deep charge/discharge of the cell with pVDF–NCC at C/1 effective rate provided 101 W h kg^{-1} to be compared with 85 W h kg^{-1} of the cell with Celgard®2400 (the cell weight was considered twice the composite electrode weight of both electrodes, as to include the contribution of all the other battery components).

HPPC tests performed at 5 C and 10 C on the cells with the two different separators to simulate the dynamic functioning of the batteries in power-assist HEVs demonstrated the superior performance of the cells with pVDF–NCC with respect to that of the cells with Celgard®2400 even if both cells exceed the FreedomCAR goals of power and energy for minimum and maximum power-assist HEV. Tests for plug-in HEV applications are in progress on cells with the new pVDF–NCC separator.

Acknowledgements

We would like to thank 7th European Framework Programme (FP7-Transport), “Advanced Fluorinated Materials for High Safety, Energy and Calendar Life Lithium Ion Batteries” (AMELIE) Project no. 265910, for financial support. Project Partners (CEA, KNUTD, SOLVAY and WWUM) are thanked for providing some cell components and for the useful discussions.

Appendix A. Supplementary material

Supplementary material related to this article can be found at http://dx.doi.org/10.1016/j.jpowsour.2013.07.095.

References

[1] K. Amine, H. Tukamoto, H. Yasuda, Y. Fujita, J. Power Sources 68 (1997) 604–608.
[2] Q. Zhong, A. Bonakdarpour, M. Zhang, Y. Gao, J.R. Dahn, J. Electrochem. Soc. 144 (1997) 205–213.
[3] T. Ohzuku, S. Takeda, M. Iwanaga, J. Power Sources 81–82 (1999) 90–94.
[4] S. Qiang, L. Xin-hai, W. Zhi-xing, J. Yong, Trans. Nonferrous Met. Soc. China 19 (2009) 176–181.
[5] S. Patoux, L. Sannier, H. Lignier, Y. Reynier, C. Bourbon, S. Jouanneau, F. Le Cras, S. Martinet, Electrochim. Acta 53 (2008) 4137–4145.
[6] S. Patoux, L. Daniel, C. Bourbon, H. Lignier, C. Pagano, F. Le Cras, S. Jouanneau, S. Martinet, J. Power Sources 189 (2009) 344–352.
[7] C. Arbizzani, F. De Giorgio, L. Porcarelli, M. Mastragostino, V. Khomenko, V. Barsukov, D. Bresser, S. Passerini, J. Power Sources 238 (2013) 17–20.
[8] C.J. Orendorff, Interface 21 (2012) 61–65.
[9] T.-H. Cho, M. Tanaka, H. Onishi, Y. Kondo, T. Nakamura, H. Yamazaki, S. Tanase, T. Sakai, J. Power Sources 181 (2008) 155–160.
[10] F. Boudin, X. Andrieu, C. Jehoulet, I.I. Olsen, J. Power Sources 82 (1999) 804–807.
[11] J. Saunier, F. Alloin, J.-Y. Sanchez, G. Caillon, J. Power Sources 119–121 (2003) 454–459.
[12] D. Djian, S. Martinet, H. Lignier, J.-Y. Sanchez, PCT WO2005/119816, U.S. Patent, US 7,642,012 B2, Jan. 5, 2010.
[13] D. Djian, F. Alloin, S. Martinet, H. Lignier, J. Power Sources 187 (2009) 575–580.
[14] J. Saunier, F. Alloin, J.-Y. Sanchez, L. Maniguet, J. Polym. Sci., Part B: Polym. Phys. 42 (2004) 2308–2317.
[15] J.-Y. Cavaillé, A. Dufresne, M. Paillet, M.A.S. Azizi-Samir, F. Alloin, J.-Y. Sanchez, WO 2004/001888 A2, U.S. Patent, US 2006/0102869 A1, May 18, 2006.
[16] INEEL, FreedomCAR Battery Test Manual for Power-assist Hybrid Electric Vehicles. Prepared for the U.S. Department of Energy, 2003.
[17] (a) Y. Molmeret, M. Bolloli, R. Scarazzini, A. Dufresne, F. Alloin, J.-Y. Sanchez, in: International Symposium on Polymer Electrolytes (ISPE-12), Selfoss (Iceland) 26–31 August 2012, Abstract pag. 126.
(b) M. Bolloli, Y. Molmeret, F. Alloin, J.-Y. Sanchez, A. Dufresne, in preparation.
[18] S.G. Stewart, V. Srinivasan, J. Newman, J. Electrochem. Soc. 155 (2008) A664–A671.